ACS APPLIED MATERIALS & INTERFACES

Research Article

www.acsami.org

Flexible, Highly Durable, and Thermally Stable SWCNT/Polyimide Transparent Electrodes

Seong-Ku Kim,[†] Tao Liu,*[,‡] and Xiaogong Wang*[,†]

[†]Department of Chemical Engineering, Laboratory of Advanced Materials (MOE), Tsinghua University, Beijing 100084, P. R. China

[‡]High-Performance Materials Institute, Florida State University, 2005 Levy Avenue, Tallahassee, Florida 32310, United States

Supporting Information

ABSTRACT: Flexible, transparent, and electrically conducting electrode materials are highly desired for flexible electronic applications. With a highly transparent polyimide (PI) as a substrate, a comprehensive and comparative study was performed to investigate four different fabrication schemes in producing transparent and electrically conducting SWCNT/PI electrodes. A very promising method that involves an in situ imidization process and nitric acid doping treatment was identified, which led to the fabrication of highly durable and thermally stable SWCNT/PI electrodes. The best performed electrode has a transmission of 77.6% at 550 nm and a sheet resistance (R_s) of 1169 ± 172 Ω/□, which appeared no changes after repeating tests of bending, folding-unfolding, adhesive-tape-peeling-off, and wet tissue-paper scratching/wiping. The excellent thermal stability of such fabricated SWCNT/PI electrode is manifested by the very high glass transition temperature of 290.1 °C and low coefficient of thermal expansion (CTE) of 28.5 ppm °C^{-1} in the temperature range from 75 to 200 °C. The new method expects to be able to pave the way in facile production of high-performance flexible, transparent, and conducting electrodes.

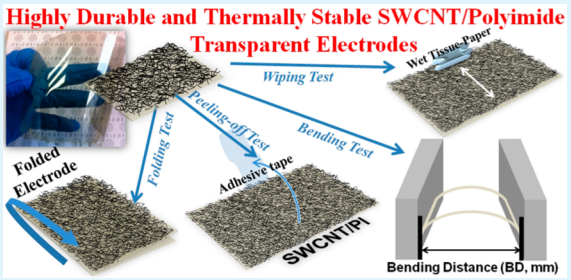

KEYWORDS: *transparent electrode, durability, thermal stability, high performance polyimide, carbon nanotube*

INTRODUCTION

Since their discovery in 1991,[1] carbon nanotubes (CNTs) have received considerable attention for applications in many fields due to their unique and outstanding properties, such as high flexibility, low mass density, and large aspect ratio.[2] To name a few, these applications include electronic transport,[3,4] integrated circuits,[5] supercapacitors,[6−9] transistors,[10−13] composites,[14−16] computer,[17] electrodes,[18−23] thermo-acoustic projectors,[24] solar cells,[25] mechanical resonators,[26] and sensor materials,[27,28] etc. Among different applications, the CNT based flexible and transparent electrodes have been a focus of recent investigations. The past efforts explored using different polymers as the substrate for CNT based flexible and transparent electrodes, such as polyurethane (PU),[16] polyethylene terephthalate (PET),[19,22−24,28] polycarbonate (PC),[23] and polydimethylsiloxane (PDMS).[18,28] Although these mentioned polymer substates have good flexibility and high transparency, they have some inherent drawbacks, e.g., low thermal and chemical stability, inferior thermomechanical properties, as well as high oxygen and mositure permeability. This may limit their use in real applications and prevent us from achieving CNT based transparent electrodes with optimized electrical conductivity, transparency, mechanical and thermo-mechanical stability and durability.

Polyimides (PIs) have good flexibility, low dielectric constant, high thermal, chemical, and mechanical stability and low permeability,[29−31] and are promising candidates for interlayer dielectrics in advanced electronic devices. In this work, we rely on a highly transparent polyimide developed in our previous work[31,32] to explore its use for facile fabrication of single-walled carbon nanotube (SWCNT) based high-performance flexible and transparent electrodes. With a wise design of the *in situ* imidization process and the SWCNT film fabrication and post-treatments, we have demonstrated a novel processing method in producing SWCNT/PI transparent and flexible electrodes. This method is able to overcome the drawbacks of the conventional approach to facilitate a strong interfacial bonding between SWCNT thin film and the insulating PI substrate. As a consequence, the newly developed SWCNT/PI flexible and transparent electrodes possess excellent durability upon repeating tests of bending, folding-unfolding, adhesive-tape-peeling-off, and wet tissue-paper scratching/wiping. The new method in combination with nitric acid doping treatment of SWCNTs allow to produce highly durable SWCNT/PI transparent electrode with a transmission of 77.6% at 550 nm and a sheet resistance (R_s) of 1169 ± 172 Ω/□. Moreover, because of the inert chemistry of PI and SWCNTs, the SWCNT/PI transparent electrodes show excellent heat-resistance and thermo-mechanical stability. It is believed that, the approach established previously by us for forming thin films

Received: July 9, 2015
Accepted: August 31, 2015
Published: August 31, 2015

DOI: 10.1021/acsami.5b06181
ACS Appl. Mater. Interfaces 2015, 7, 20865−20874

of transparent linear polyimide[32] as well as the novel method developed in this work for fabricating durable and highly transparent and electrical conductive SWCNT/PI electrodes, would be able to pave the way in facile production of high-performance flexible and transparent electrodes, which may find a broad range of applications in flexible electronics, such as, organic light-emitting diodes (OLEDs), thin film transistors (TFTs), liquid crstyal (LCDs), and eletrophoresis displays.[33]

EXPERIMENTAL SECTION

Materials. 4, 4′-(Hexafloroisopropylidene) diphthalic anhydride (6FDA, 95%) and 2, 2′-bis(trifluoromethyl) benzidine (TFDB, 98%) were purchased from Adamas-Reagent Co. Ltd. 4, 4′-Bis(3-aminophenoxy) diphenylsulfone (mBAPS, 98%) was purchased from Tokyo Chemical Industry Co. Ltd. (TCI). Sodium dodecylbenzenesulfonate (SDBS) was purchased from Sigma-Aldrich. The solvent *N*-methyl-2-pyrrolidone (NMP, 97%) and nitric acid were purchased from Beijing Modern East Fine Chemical. Purified single-walled carbon nanotube raw materials (HiPco SWCNT) were purchased from Carbon Nanotechnologies Inc. (PO # 355) and used as-received. If not mentioned specifically, the chemicals and solvents were used as received without further purification.

Preparation of Flexible and Transparent SWCNT/PI Electrodes. The transparent linear polyimide ($PI_{6FDA\text{-}TFDB\text{-}mBAPS}$) was synthesized by a traditional two-step condensation method according to the procedures disclosed in our previous work.[31] The aqueous dispersion of SWCNTs was prepared by sonicating and centrifuging a mixed solution of 16 mg SWCNTs in 100 mL of deionized water (DI water, H_2O) with 0.7 wt % SDBS. The preparation and characterization details of SWCNT/SDBS dispersion have been previously described.[28,34−36] With the previously developed PI synthesis method, we have attempted four different approaches (S1a−S1d) to fabricate SWCNT/PI electrodes, which are shown in Scheme 1.

Scheme 1. Sketched Procedures for Preparing Transparent SWCNT/PI Electrodes by Using Four Different Fabrication Schemes S1a−S1d

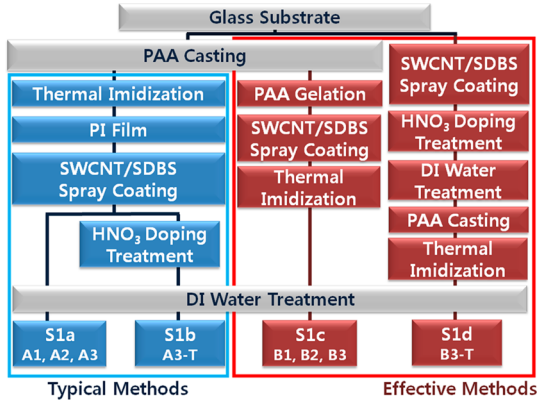

In the scheme of S1a, a thin film of PI was first formed on a glass substrate by a thermal imidization process.[32] Subsequently, a certain amount of SWCNT/SDBS dispersion was sprayed onto the formed PI film, which was heated by a hot plate (JF-956A, JFTOOIS) to 110 °C to accelerate water evaporation and facilitate the formation of a thin SWCNT/SDBS film. The spray was carried out with Iwata HI-LINE HP-CH air brush operated at 200 kPa. In the spray process, the spray region was confined to a predetermined area such that the finally formed SWCNT/SDBS film had a 10 cm × 10 cm square shape. To remove the residual SDBS molecules, the as-formed PI_SWCNT/SDBS film was further subjected to immersion treatment in DI water for 24 h and then dried in air at ambient temperature to result in the SWCNT/PI electrode. With scheme S1a, we varied the amount of SWCNT/SDBS dispersion at 7, 14, and 21 mL and respectively prepared A1, A2, and A3 SWCNT/PI electrodes with increased SWCNT thin film thickness and packing density.

The scheme of S1b is similar to S1a. The only difference is that the as-formed PI_SWCNT/SDBS film was first treated by nitric acid for 20 min and then subjected to immersion treatment in DI water for 24 h. With S1b scheme and an amount of 21 mL of SWCNT/SDBS dispersion, the A3-T SWCNT/PI electrode was prepared for comparison with A3 sample to examine the effect of nitric acid doping.

In scheme S1c, a partially gelated polyamic acid (PAA) film was prepared first by casting the PAA precursor on a glass plate and then heated at 100 °C for 2 h. Following the formation of PAA film, a certain amount of dispersion was sprayed to form a layer of SWCNT/SDBS. A stepwise thermal imidization (150 °C for 1 h, 200 °C for 1 h, and 300 °C for 1 h) was then subsequently applied to give PI_SWCNT/SDBS film. The SWCNT/PI electrode was finally formed upon immersion treatment of the as-prepared PI_SWCNT/SDBS film in DI water for 24 h and drying in air at ambient temperature. With the scheme S1c, we respectively prepared B1, B2, and B3 SWCNT/PI electrodes with increased SWCNT thin film thickness and packing density by spraying 7, 14, and 21 mL of SWCNT/SDBS dispersion.

In schemes of S1a, S1b, and S1c, the SWCNT/SDBS film was formed on either a PI film or a PAA film. In contrast to this, in scheme S1d, the SWCNT film was formed on a glass substrate first. This was done by spraying 21 mL of SWCNT/SDBS dispersion on a heated glass substrate (110 °C). Subsequent to nitric acid doping for 20 min and a DI water immersion treatment for 24 h, the SWCNT film was formed upon drying in air at ambient temperature. Following the formation of SWCNT/PI electrode, the PAA precursor was then cast on the SWCNT layer and maintained at 80 °C for 2 h to result in a PAA_SWCNT film. A similar stepwise thermal imidization process as used in S1c was finally applied to give the B3-T SWCNT/PI electrode.

As noted, all the SWCNT/PI electrodes prepared by different schemes were supported on a glass substrate. The free-standing film can be readily obtained by sonicating the supported film in hot DI water at 80 °C and a subsequent drying process in air at ambient temperature.

Characterization and Test of Transparent and Conducting SWCNT/PI Electrodes. The morphologies of the SWCNT/PI electrodes were examined by scanning electron microscopy (SEM) using a S5500 microscope (Hitachi) operating at an acceleration voltage of 5.0 kV. The samples were sputter coated with carbon before imaging. To visualize the cross-section morphology, we fractured the film specimen in liquid nitrogen. For selected samples, the energy dispersive spectroscopy (EDS) was performed by field emission scanning electron microscope (FE-SEM) using a Carl Zeiss MERLIN equipment operating at an acceleration voltage of 5.0 kV to determine the presence of residual SDBS molecules. X-ray photoelectron spectroscopy (XPS, Thermo ESCALAB 250Xi) measurement was also performed for the same purpose. Thermal gravimetric analysis (TGA) was performed with a TGA 2050 analyzer (TA Instruments Co.) at a heating rate of 20 °C from room temperature to 900 °C under nitrogen to examine the thermal stability of the prepared PI and SWCNT/PI films. The glass transition temperature (T_g) of the PI polymer was determined by differential scanning calorimeter (DSC 2910, TA Instrument Co.) with a heating rate of 20 °C min^{-1} under nitrogen. The in-plane coefficient of thermal expansion (CTE) of the PI or SWCNT/PI films was measured using a dynamic mechanical analyzer (Q800 DMA, TA Instrument Co.) in extension mode over a temperature range from 25 to 220 °C with a force of 0.01 N. The size of specimens was 14 mm in length, 5 mm in width, and 22−27 μm in thickness.

The current versus voltage (I−V) characteristics of the SWCNT/PI electrodes prepared by all four different schemes were measured at room temperature using a Keithley 236 source unit. For electrical measurements, silver conductive paint was applied to prepare the 2-proble testing electrodes for evaluating the I−V behavior of different SWCNT/PI electrodes and determining the sheet resistance R_s (Ω/□). The typical size of the specimen used for sheet resistance measurement was 2 cm × 2 cm in square shape. For rectangular

DOI: 10.1021/acsami.5b06181
ACS Appl. Mater. Interfaces 2015, 7, 20865−20874

sample of width (W) and length (L), the R_s was calculated according to $R_s = R\ (W/L)$, where R is the sample resistance. UV−visible absorption spectra of the supported SWCNT/PI electrode were acquired by using a Lamba Bio-40 spectrometer (Perkin−Elmer) with a silica glass plate as the reference.

RESULTS AND DISCUSSION

Optical Transmission, Morphology, and X-ray Photoelectron Spectroscopy (XPS) Analysis of SWCNT/PI Electrodes. The optical transmission spectra of all the SWCNT/PI electrodes prepared by S1a−S1d are shown in Figure 1. In the same figure, the spectrum of a neat PI film is also shown for comparison. Table 1 lists the cutoff wavelengths (absorption edge, λ_{cutoff}) and the transmission at 550 nm for all films. Without SWCNT coating, the pristine PI shows the highest transmission of 98.8% at 550 nm and it is colorless in the visible region. The extremely high transmission of the PI synthesized in this work has been attributed to the rigid, kinked, and distorted molecular structures in the backbone.[32] Such a structure effectively inhibits the dense packing of polymer chains and therefore the inter- and intrachain π-electron transfer between benzene and imide rings that commonly occur in the conventional PI to result in high transparency. After forming an optically absorbing SWCNT layer on PI, the transmission of the SWCNT/PI electrodes was gradually decreased with increasing the amounts of deposited SWCNTs. With increasing the spraying amount of SWCNT/SDBS dispersion from 7 to 21 mL, which basically increases the thickness and SWCNT packing density of the finally formed SWCNT layer, the transmission of the SWCNT/PI film obtained by scheme S1a decreased from 92.9% (A1) to 76.1% (A3). Similar results were obtained for the SWCNT/PI films prepared by scheme S1c (93.3% for 7 mL (B1) and 75.5% for 21 mL (B3)). The fabrication scheme-independent optical transmission of SWCNT/PI electrode was further manifested through the sample A3-T (77.4% at 550 nm) and B3-T (77.6% at 550 nm), which were respectively prepared by S1b and S1d with 21 mL of SWCNT/SDBS dispersion. The morphologies of the SWCNT/PI electrodes prepared by different fabrication schemes were examined by scanning electron microscopy (SEM). The results are shown in Figure 2. Despite the different fabrication schemes, all films show a common entangled SWCNT network morphology. With increasing the amount of SWCNT/SDBS dispersion from 7 to 21 mL, the packing density of SWCNTs accordingly increases in A1−A3 and in B1−B3 (Figure 2a). This is in accordance with the transmission trend observed in Figure 1. Upon comparison of the SEM

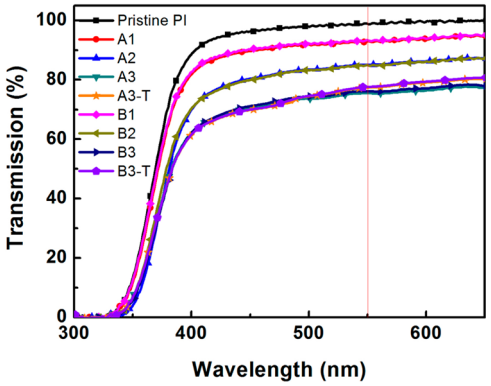

Figure 1. UV−vis transmission spectra of the pristine PI and SWCNT/PI electrodes prepared by schemes S1a−S1d.

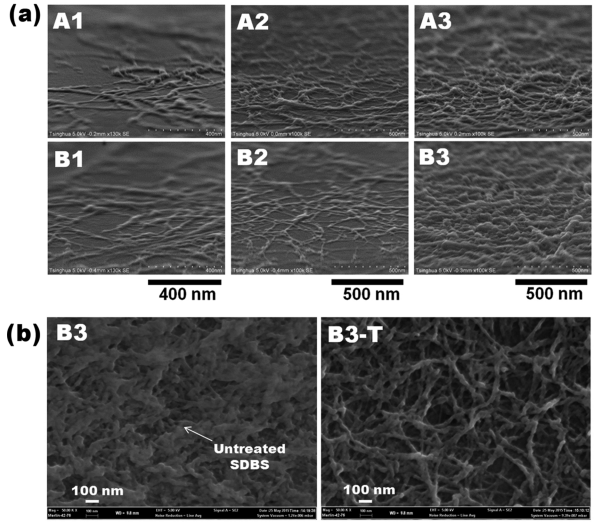

Figure 2. SEM images of (a) the cross-section of the SWCNT/PI electrodes prepared by spraying (A1, B1) 7, (A2, B2) 14, and (A3, B3) 21 mL of SWCNT/SDBS dispersion, and (b) the top surface of the SWCNT/PI electrodes prepared by scheme S1c(B3) and S1d(B3-T).

Table 1. Sheet Resistance (R_s), Transmission, and Thermal Properties of Pristine PI and SWCNT/PI Electrodes

	transmission		sheet resistance[a]		DSC	TGA		
sample	λ_{cutoff} (nm)	@550 nm (%)	R_s (Ω/□)	3D VRH T_o[b] (K)	T_g (°C)	$T_d^{5\%}$[c] (°C)	R_{w800}[d] (%)	CTE[e] (ppm °C^{-1})
pristine PI	327	98.8			284.1	539.8	48.3	33.9
A1	324	92.9	5186 ± 734	29725 ± 8250	284.2	543.2	49.6	32.9
A2	327	85.1	2903 ± 411	34503 ± 9766	284.1	543.5	51.3	32.6
A3	327	76.1	1914 ± 271	37732 ± 10651	284.1	543.3	52.6	32.2
A3-T	327	77.4	1229 ± 181	26966 ± 7847	284.1	543.8	52.5	32.4
B1	325	93.3	51547 ± 7600	127334 ± 36673	286.1	543.1	49.9	32.4
B2	327	84.9	24012 ± 3466	137537 ± 39119	288.6	543.2	51.3	31.5
B3	328	75.5	10145 ± 1434	113790 ± 31874	290.1	543.6	52.6	29.9
B3-T	327	77.6	1169 ± 172	26012 ± 7433	293.2	544.2	52.4	28.5

[a]Sheet resistances were measured by KEITHLEY at room temperature. [b]Mott characteristic temperature for a conducting material that obeys 3-dimensional variable range hopping (3D VRH) transport mechanism. [c]Weight loss temperatures at 5 and 10 wt % were recorded by TGA at a heating rate of 20 °C min^{-1} and a N_2 gas flow rate of 25 cm^3 min^{-1}. [d]Weight residue at 800 °C. [e]The temperature range from 75 to 200 °C with a force of 0.01 N.

DOI: 10.1021/acsami.5b06181
ACS Appl. Mater. Interfaces 2015, 7, 20865−20874

images of B3 and B3-T (Figure 2b), the presence of enriched SDBS phase in the former sample is evident. It is believed that the nitric acid treatment process used for preparing B3-T in scheme S1d, which was lacking in preparing B3 (scheme S1c), could effectively remove the residual SDBS surfactants and therefore enhance the optical and electrical properties of the SWCNT/PI electrodes. The slightly increased transmission of B3-T as compared to B3 (Figure 1) seems in line with this argument. The EDS and XPS were performed to further examine the SDBS contents in B3 and B3-T. Figure 3a, b,

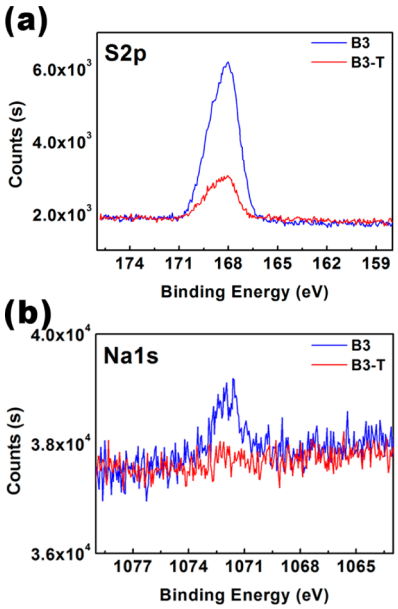

Figure 3. Comparison of the XPS binding energy spectra for the SWCNT/PI electrodes prepared by scheme S1c (B3) and S1d (B3-T). (a) 2p electron of sulfur, S 2p; and (b) 1s electron of sodium, Na 1s.

respectively, compares the XPS binding energy spectra of sulfur (S 2p) and sodium (Na 1s), which exist only in SDBS. Clearly, upon nitric acid doping treatment for 20 min, the atomic contents of sulfur and sodium in B3-T were significantly reduced as compared to that in B3 sample. Similar conclusions can also be derived from the EDS results (Figure S2). The experimental evidence provided by EDS and XPS both suggest that the nitric acid treatment is efficient in removing the residual SDBS surfactants to impart the SWCNT/PI electrode with good electrical conductivity, high durability, and good mechanical stability.

The results shown in Figure 1 and 2 all suggest that the optical transmission and SEM morphologies of SWCNT/PI electrodes have no or negligible dependence on sample preparation schemes. This is in drastic contrast to the electrical property of SWCNT/PI electrodes, which strongly depends upon the fabrication schemes as discussed below.

Electrical Performance Evaluation of SWCNT/PI Electrodes. Figure 4a, b compares the voltage versus current behavior for all the SWCNT/PI electrodes, which indicate that all samples are omhic. Figure 4c, d compare the sheet resistance (R_s) vs the transmission (550 nm) for all samples, and the results are also summarized in Table 1.

Figure 4c, d compares the samples respectively prepared by S1a and S1b at varied amounts of SWCNT/SDBS dispersion. With increasing the spraying amount from 7 to 21 mL, a monotonically decreasing trend is clearly borne out for both the sheet resistance (R_s) and optical transmission. In addition, at comparable transmission, the sheet resistance (R_s) for the samples prepared by S1c is more than one order of magnitude higher than the one prepared by S1a. This observation has been attributed to that the process in S1c, first forming SWCNT film followed by thermal imidization, may lead to high contact resistance due to the impregnation of PI into SWCNT network as well as the relatively high concentration of residual SDBS. In comparison to the series samples of A1 to A3, the sheet resistance (R_s) of the series sample B1 to B3 is much higher. The sheet resistance (R_s) for A1 and A3 is respectively 5186 ± 734 Ω/□ and 1914 ± 271 Ω/□; but it is 51547 ± 7600 Ω/□ and 10145 ± 1434 Ω/□ for B1 and B3, respectively. Among the samples A3, B3, A3-T, and B3-T, which were prepared by using the same amount of SWCNT/SDBS dispersion (21 mL) but different fabrication schemes, the ones experienced nitric acid doping treatment, A3-T (R_s = 1229 ± 181 Ω/□) and B3-T (R_s = 1169 ± 172 Ω/□), show much lower sheet resistance. This suggests that nitric acid treatment has an effect to reduce the sheet resistance (R_s) through effectively removing the residual SDBS molecules and therefore improving the van der Waals' interactions among SWCNTs. Certainly, another major factor for the enhanced electrical conductivity is due to the doping effect of nitric acid, which causes p-type doping of SWCNT by NO_3^- to introduce additional charge carriers and therefore enhance the electrical conductivity of SWCNTs.[37]

The quantity σ_{ac}/σ_{dc} – the ratio of the optical conductivity to the DC conductivity has been suggested as a good quality indicator for evaluating the performance of SWCNT films as transparent and conducing material.[38] The smaller is the σ_{ac}/σ_{dc}, the better is the performance. Our recent work has established the 3D VRH (variable range hopping) as the charge transport mechanism in SWCNT thin films prepared at different processing conditions.[39] In 3D VRH, the key parameter to characterize the charge transport behavior is T_0, the Mott characteristic temperature, which depends upon the electronic density of the (localized) states at the Fermi level – $N(E_F)$ and the localization length of the electronic wave functions ξ by $T_0 \propto \xi^{-3} N(E_F)^{-1}$. Qualitatively, the higher is $N(E_F)$ and the longer is ξ and therefore the smaller is T_0, the more easy for the charge carriers to transport. For SWCNT thin films, our previous work has established a power law relation between T_0 and σ_{ac}/σ_{dc} as $T_0 = 968.4 \times (2\pi/c \times \sigma_{ac}/\sigma_{dc})^{0.65}$. As such, the strong correlation between T_0 and σ_{ac}/σ_{dc} suggests that one can use not only σ_{ac}/σ_{dc} but also T_0 as the quality indicator for evaluating the transparent and conducting performance of SWCNT thin films. To better evaluate the effect of different processing schemes on the performance of SWCNT/PI electrodes, the σ_{ac}/σ_{dc} as well as T_0 were evaluated for all the samples, and the results are respectively shown in Figure 4e, f. In terms of both quality indicators, σ_{ac}/σ_{dc} and T_0, one can immediately identify that the SWCNT/PI electrodes prepared by S1c schemes are inferior to those prepared by S1a, S1b, and S1d. Within the experimental errors, the quality indicators of σ_{ac}/σ_{dc} and T_0 for the series samples prepared by S1a seem to show a slightly deteriorated trend with increasing the amount of SWCNT/SDBS dispersion being used in the spraying process. This is evidenced by a relatively lower value of T_0 for A1 (29725 ± 8250 K) as compared to that for A3 (37732 ± 10651 K). On the basis of the values of σ_{ac}/σ_{dc} or T_0 for A3, A3-T, B3, and B3-T, all of which were prepared with the same amount of SWCNT dispersion (21 mL) but respectively fabricated by S1a, S1b, S1c, and S1d, we can rank the four

DOI: 10.1021/acsami.5b06181
ACS Appl. Mater. Interfaces 2015, 7, 20865−20874

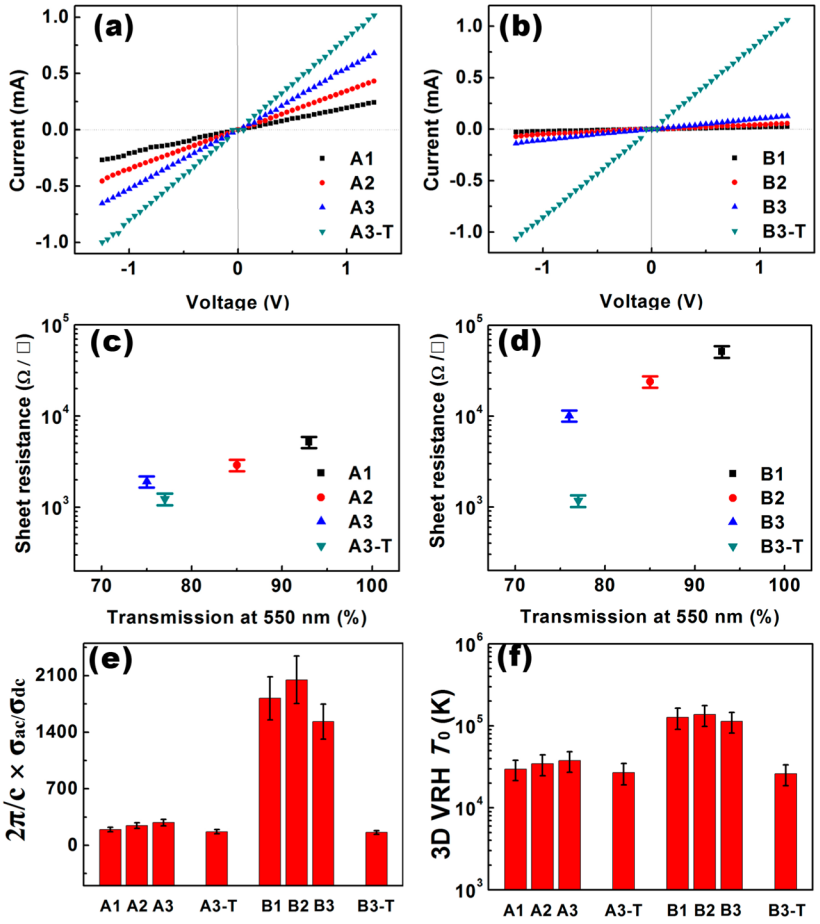

Figure 4. Comparison of (a, b) voltage versus current, (c, d) transmission at 550 nm versus sheet resistance (R_s), and (e) ratio of the optical conductivity to DC conductivity, σ_{ac}/σ_{dc}, and (f) the 3D VRH parameter Mott temperature T_0 for the SWCNT/PI electrodes prepared by different fabrication schemes.

different fabrication schemes as S1b ≈ S1d > S1a ≫ S1c. The nitric acid doping treatment applied in both S1b and S1d is believed to be responsible for the resulting SWCNT/PI electrodes with good transparent and conducting quality or low T_0, 26966 ± 7847 K for A3-T and 26012 ± 7433 K for B3-T. As discussed next, the nitric acid doping treatment in combination with in situ thermal imidization has imparted the B3-T sample with not only good transparent and conducting quality but also excellent durability.

Durability of SWCNT/PI Electrodes as Transparent and Conducting Films. In addition to transmission and electrical conductivity, the durability is also the key consideration in order for the SWCNT/PI electrodes to be useful for practical transparent and conducting material application. With sheet resistance (R_s) change as a quality-control parameter, a few different tests, which include bending, folding-unfolding, adhesive-tape peeling-off, and tissue-paper-scratching, were performed to identify the best fabrication scheme that allows for the optimization of the durability of SWCNT/PI electrodes. The schematics of the bending test are shown in Figure 5 and the testing results are listed in Table 2. Upon varying the end-to-end distance of the test specimen from 15 to 1 mm to gradually increase the bending curvature, the samples prepared by four different fabrication schemes all showed negligible changes on the sheet resistance (R_s). No visible cracks or failure was observed for all the test specimens after the bending test.

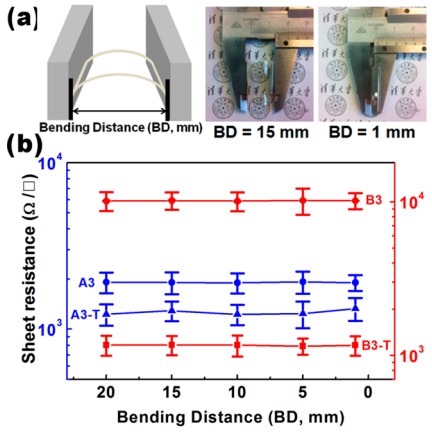

Figure 5. (a) Photographs of the bending test schematics and procedures. The end-to-end distance of the bent film is used as a measure for the bending curvature. (b) Effect of bending curvature on the sheet resistance (R_s).

To further evaluate the bending performance of the SWCNT/PI electrodes, repeating folding-unfolding test was applied. The results are shown in Figure 6 and listed in Table 3. Upon 100 times of folding-unfolding, the samples prepared by both S1c (B-3) and S1d (B3-T) exhibited excellent stability. The sheet resistance (R_s) maintained unchanged when compared with the pristine value. In contrast, the electrical

DOI: 10.1021/acsami.5b06181
ACS Appl. Mater. Interfaces 2015, 7, 20865−20874

Table 2. Comparison of Bending Test on the Sheet Resistance (R_s) Results of A3, A3-T, B3, and B3-T

	sheet resistance (R_s, Ω/□)				
	flat state			bending test	
sample	L^a = 20 mm	BD[b] = 15 mm	BD = 10 mm	BD = 5 mm	BD = 1 mm
A3	1914 ± 271	1908 ± 289	1899 ± 265	1923 ± 291	1903 ± 209
A3-T	1229 ± 181	1291 ± 175	1227 ± 171	1239 ± 227	1330 ± 210
B3	10145 ± 1434	10215 ± 1325	10132 ± 1432	10239 ± 1998	10191 ± 1240
B3-T	1169 ± 172	1170 ± 166	1168 ± 181	1151 ± 139	1165 ± 168

[a]Sample length of regular quadrilateral. [b]Bending distance of the samples.

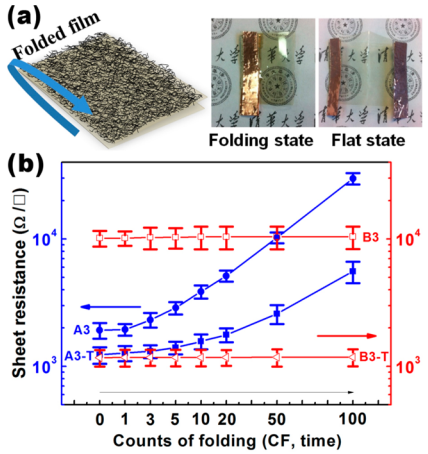

Figure 6. (a) Photographs of the folding-unfolding test procedures. (b) Effect of repeating folding-unfolding test on the sheet resistance (R_s).

performance for the samples prepared by S1a (A3) and S1b (A3-T) both deteriorated significantly upon repeating folding and unfolding test. After 100 times test, an about 5-fold and 20-fold increase on the sheet resistance (R_s) have been respectively observed for A3-T (from 1229 ± 1811 Ω/□ to 5563 ± 181 Ω/□) and A-3 (from 1914 ± 271 Ω/□ to 29863 ± 3015). The influence of the externally applied mechanical strain on the microstructures and therefore the electrical properties of SWCNT thin film has been studied in depth in the work by Hobbie et al. and Zhao et al.[40,41] It was found that the strain-induced changes in microstructure and percolation threshold would affect the elasticity and sheet resistance of SWCNT thin films. However, this has not been the case for the thin films prepared by the schemes **S1c** and **S1d**, which show excellent durability upon cyclic strain test. Here we attribute two mechanisms that are responsible for the durability of the SWCNT thin film prepared by the schemes **S1c** and **S1d**. First, the SWCNT networks being studied here is well above the percolation threshold. As compared to the network nearby the percolation region, the network structure of our thin film is well developed and stronger and possesses the enhanced capability to resist the external mechanical deformation. Second, in the schemes of **S1c** and **S1d**, a thermal imidization process has been involved after the SWCNT network formation, which facilitates a strong adhesion between SWCNT layer and the PI substrate to result in stronger and more robust thin film samples (B-3 and B3-T) with excellent durability. In contrast, this second mechanism is lacking in the thin films prepared by **S1a** and **S1b**, where the SWCNT layer was directly deposited on a PI substrate. This leads to a relatively weak interfacial bonding between SWCNT layer and the PI substrate for A-3 and A3-T samples and therefore inferior performance in cyclic folding-unfolding test.

The excellent durability of the SWCNT/PI electrodes prepared by the schemes **S1c** and **S1d** was further demonstrated through adhesive-tape-peeling-off test. The results are shown in Figure 7 and listed in Table 4. As expected, after repeating peeling-off tests, the sheet resistance R_s of B3 and B3-T maintained the pristine value respectively as $R_{s,\ CP=5}$ = 10292 ± 1344 Ω/□ and $R_{s,\ CP=5}$ = 1164 ± 167 Ω/□, and the SEM images show intact SWCNT network morphology. In contrast, the SWCNT layer in A3 prepared by **S1a** was completely removed from the PI substrate after

Table 3. Comparison of the Repeating Folding-Unfolding Test on the Sheet Resistance (R_s) Results of A3, A3-T, B3, and B3-T

	sheet resistance (R_s, Ω/□)			
	flat state		folding-unfolding test	
sample	CF[a] = 0	CF = 1	CF = 3	CF = 5
A3	1914 ± 271	1942 ± 204	2315 ± 302	2876 ± 321
A3-T	1229 ± 181	1270 ± 173	1309 ± 149	1400 ± 161
B3	10145 ± 1434	10149 ± 1325	10285 ± 2009	10299 ± 1893
B3-T	1169 ± 172	1173 ± 175	1176 ± 168	1173 ± 172
	sheet resistance (R_s, Ω/□)			
	folding−unfolding test			
sample	CF = 10	CF = 20	CF = 50	CF = 100
A3	3862 ± 458	5126 ± 513	10233 ± 996	29863 ± 3015
A3-T	1568 ± 209	1767 ± 221	2582 ± 435	5563 ± 1065
B3	10391 ± 2105	10402 ± 2098	10406 ± 2113	10416 ± 2106
B3-T	1174 ± 174	1175 ± 164	1177 ± 181	1179 ± 179

[a]The counts of sample folding test.

DOI: 10.1021/acsami.5b06181
ACS Appl. Mater. Interfaces 2015, 7, 20865−20874

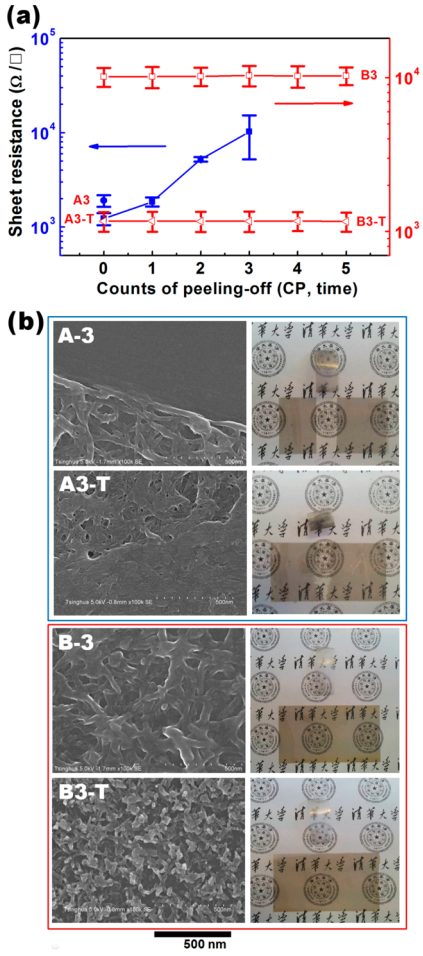

Figure 7. (a) Effect of repeating adhesive-tape-peeling-off test on the sheet resistance (R_s), and (b) SEM images and photographs of the samples after peeling-off test.

only once detaching test. The A3-T that was prepared by **S1b** showed a slightly better performance. It failed after three times of detaching test. The nitric acid doping treatment in **S1b** used for preparing A3-T seems helpful in improving the van der Waals' interactions among the SWCNTs by effectively removing the residual SDBS and therefore a better durability performance. This has been confirmed by a wet tissue-paper scratching/wiping test conducted for A3, A3-T, B3, and B3-T samples. The results are shown in Figure 8 and listed in Table 5. Similar to the adhesive-tape-peeling-off test, the A3 sample failed after only once wiping test. A slightly better performance was observed for A3-T sample. With increasing the times of wiping, the sheet resistance R_s of A3-T rapidly increased until completely failed after three times wiping. The wiping test also

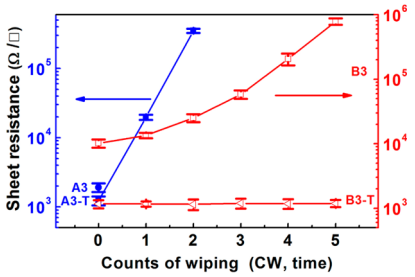

Figure 8. Effect of wet tissue-paper scratching/wiping test on the sheet resistance (R_s).

resulted in performance deterioration for B3 sample. After five times repeating wiping tests, the sheet resistance R_s of B3 continuously increased from the original value of $R_{s,\ CW=0}$ = 10145 ± 1434 Ω/□ to $R_{s,\ CW=5}$ = 788240 ± 88691 Ω/□. The performance deterioration upon tissue-paper scratching/wiping test has not been observed for B3-T, which maintained the pristine value at $R_{s,\ CW=5}$ = 1192 ± 153 Ω/□. The combination of nitric acid doping treatment and thermal imidization involved in **S1d** lead to the best performed B3-T sample. The former process facilitates a high-efficiency removal of SDBS and p-type doping to result in low sheet resistance; and the latter procedure allows the adhesion/impregnation of SWCNTs in PI matrix that imparts a strong interfacial bonding between SWCNTs and the PI substrate and therefore the excellent durability.

Thermal Stability Characterization of SWCNT/PI Electrodes. Among different performance criteria, the thermal stability is also important for transparent and conducting electrodes in the relatively high-temperature applications, e.g., organic solar cells.[42] To this regard, we have used DSC to characterize the glass transition behavior of the SWCNT/PI electrodes prepared by different fabrication schemes. The results are shown in Figure 9a, b and summarized in Table 1. As compared to the pristine PI, which has a glass transition temperature (T_g) of 284.1 °C, the different fabrication schemes resulted SWCNT/PI electrodes did not show any thermal stability deterioration. The SWCNT/PI electrodes prepared by S1a (A1, A2, and A3) and S1b (A3-T) SWCNT/PI electrodes showed comparable T_g values ranging from 284.1 to 284.2 °C. Even better, an enhanced T_g has been observed for the SWCNT/PI electrodes prepared by S1c (B1, B2, and B3, ranging from 286.1 to 290.1 °C) and S1d (B3-T, 290.1 °C).

Figure 9c, d compares the temperature-dependent thermal expansion behavior for the pristine PI and SWCNT/PI electrodes. The corresponding results of the coefficient of thermal expansion (CTE) are listed in Table 1. In consistent with the T_g results shown in Figure 9a, b, the CTEs for the SWCNT/PI electrode prepared by S1a and S1b are comparable

Table 4. Comparison of Repeating Adhesive-Tape-Peeling-off Test on the Sheet Resistance (R_s) Results of A3, A3-T, B3, and B3-T

	sheet resistance (R_s, Ω/□)					
sample	CP[a] = 0	CP = 1	CP = 2	CP = 3	CP = 4	CP = 5
A3	1914 ± 271	[b]				
A3-T	1229 ± 181	1857 ± 211	5231 ± 305	10253 ± 5014		
B3	10145 ± 1434	10152 ± 1591	10210 ± 1397	10328 ± 1569	10249 ± 1631	10292 ± 1344
B3-T	1169 ± 172	1172 ± 174	1168 ± 175	1170 ± 177	1173 ± 165	1164 ± 167

[a]The counts of samples peeling-off test. [b]Nonconductive state.

DOI: 10.1021/acsami.5b06181
ACS Appl. Mater. Interfaces 2015, 7, 20865−20874

Table 5. Comparison of Repeating Wet Tissue-Paper Scratching/Wiping Test on the Sheet Resistance (R_s) Results of A3, A3-T, B3, and B3-T

	sheet resistance (R_s, Ω/□)					
sample	CW[a] = 0	CW = 1	CW = 2	CW = 3	CW = 4	CW = 5
A3	1914 ± 271	[b]				
A3-T	1229 ± 181	19733 ± 1732	351204 ± 24636			
B3	10145 ± 1434	13524 ± 1304	25150 ± 3471	58207 ± 8720	206329 ± 43016	788240 ± 88691
B3-T	1169 ± 172	1170 ± 105	1153 ± 214	1197 ± 211	1183 ± 198	1192 ± 153

[a]The counts of sample wiping test. [b]Nonconductive state.

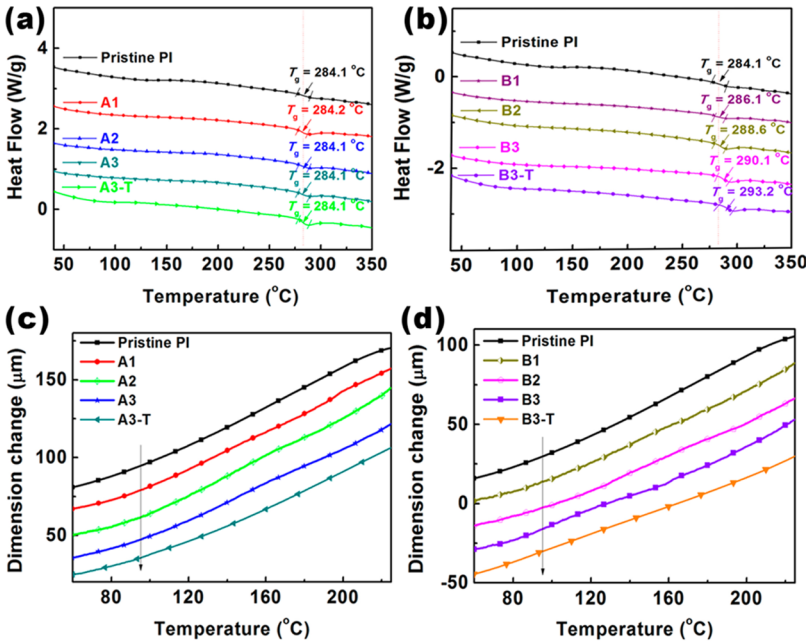

Figure 9. Thermal stability results of the SWCNT/PI thin films examined by (a, b) differential scanning calorimetry (DSC) for heat flow and (c, d) dynamic mechanical analysis (DMA) for temperature-dependent dimension change.

Table 6. Qualitative Summary on the Performance of SWCNT/PI Electrodes Prepared by Four Different Fabrication Schemes: S1a for of A3; S1b for A3-T; S1c for B3; and S1d for B3-T

	property					durability		
sample	T_r[a]	R_s[b]	3D VRH T_0[c]	TS[d]	$R_{s,BD}$[e]	$R_{s,CF}$[f]	$R_{s,CP}$[g]	$R_{s,CW}$[h]
A3	good	good	fair	good	good	poor	poor	poor
A3-T	good	good	good	good	good	poor	poor	poor
B3	good	poor	poor	good	good	good	good	poor
B3-T	good	good	good	good	good	good	good	good

[a]Transmission. [b]Sheet resistance. [c]Mott characteristic temperature. [d]Thermal stability. [e]Bending test. [f]Folding-unfolding test. [g]Peeling-off test. [h]Wiping test.

to that of the pristine PI. The schemes S1c and S1d lead to a reduced CTE. In the temperature range from 75 to 200 °C, the CTE decreased from 33.9 ppm $°C^{1-}$ for the pristine PI to 28.5 ppm $°C^{-1}$ for the B3-T sample. The strong interfacial bonding between SWCNT layer and the PI substrate caused by the in situ thermal imidization process involved in S1c and S1d has been attributed to be the key factor for the enhanced thermal stability (higher T_g and lower CTE) of B1, B2, B3, and B3-T. As compared to the different polymer substrates used for developing flexible, transparent and conducting electrodes, e.g., polyurethane (PU, T_g ~ 60 to 139 °C; CTE ~ 30 to 70 ppm $°C^{1-}$), polyethylene terephthalate (PET, T_g ≈ 67 to 81 °C; CTE ~ 70 ppm $°C^{1-}$) and polydimethylsiloxane (PDMS, T_g ≈ −111 to −120 °C; CTE ≈ 310 ppm $°C^{-1}$, the SWCNT/PI electrodes developed here show much superior thermal stability in terms of low CTE and high T_g.

CONCLUSION

Four different schemes were applied to fabricate SWCNT/PI film based transparent and conducting electrodes. The effect of different fabrication schemes on the electrical property, optical transmission, mechancial durability, and thermal stability of SWCNT/PI electrode were comphrehensively evaluated, characterized and compared. Table 6 qualitatively summerizes and compares the performance of the SWCNT/PI electrodes fabricated by different schemes. Among the different schemes being investigated, a very promising process, which involves in situ thermal imidization in combination with nitric acid doping

DOI: 10.1021/acsami.5b06181
ACS Appl. Mater. Interfaces 2015, 7, 20865−20874

treatment, has been identified. This method leads to transparent and conductive SWCNT/PI electrodes with excellent mechanical durability and thermal stability, which are superior to the electrodes based on polyurethane (PU), polyethylene terephthalate (PET), polydimethylsiloxane (PDMS), etc. The novel method developed in this work for fabricating durable and highly transparent and electrical conductive SWCNT/PI electrodes expects to be able to pave a way in facile production of high-performance flexible and transparent electrodes.

■ ASSOCIATED CONTENT

Supporting Information

It includes more characterization results on the scanning electron microscope (SEM) images, optical photographs, elemental spectra, and the thermal decomposition temperatures (TGA) of various SWCNT/PI thin films. The Supporting Information is available free of charge on the ACS Publications website at DOI: 10.1021/acsami.5b06181.

(PDF)

■ AUTHOR INFORMATION

Corresponding Authors

*E-mail: liutao@eng.fsu.edu.

*E-mail: wxg-dce@mail.tsinghua.edu.cn.

Notes

The authors declare no competing financial interest.

■ ACKNOWLEDGMENTS

The financial support from National Basic Research Program of China (973 Program) under Project 2011CB606102 and Tsinghua global scholars fellowship program are gratefully acknowledged.

■ REFERENCES

(1) Ijima, S. Helical Microtubelues of Graphitic Carbon. *Nature* **1991**, *354*, 56−58.

(2) Spitalsky, Z.; Tasis, D.; Papagelis, K.; Galiotis, C. Carbon Nanotube−Polymer Composites: Chemistry, Processing, Mechanical and Electrical Properties. *Prog. Polym. Sci.* **2010**, *35*, 357−401.

(3) Xie, W.; Prabhumirashi, P. L.; Nakayama, Y.; McGarry, K. A.; Geier, M. L.; Uragami, Y.; Mase, K.; Douglas, C. J.; Ishii, H.; Hersam, M. C.; Frisbie, C. D. Utilizing Carbon Nanotube Electrodes to Improve Charge Injection and Transport in Bis(trifluoromethyl)-dimethyl-rubrene Ambipolar Single Crystal Transistors. *ACS Nano* **2013**, *7*, 10245−10256.

(4) Novaes, F. D.; Rurali, R.; Ordejón, P. Electronic Transport between Graphene Layers Covalently Connected by Carbon Nanotubes. *ACS Nano* **2010**, *4*, 7596−7602.

(5) Sun, D.; Timmermans, M. Y.; Tian, Y.; Nasibulin, A. G.; Kauppinen, E. I.; Kishimoto, S.; Mizutani, T.; Ohno, Y. Flexible High-Performance Carbon Nanotube Integrated Circuits. *Nat. Nanotechnol.* **2011**, *6*, 156−161.

(6) Fan, X.; Yu, C.; Ling, Z.; Yang, J.; Qiu, J. Hydrothermal Synthesis of Phosphate-Functionalized Carbon Nanotube-Containing Carbon composites for Supercapacitors with Highly Stable Performance. *ACS Appl. Mater. Interfaces* **2013**, *5*, 2104−2110.

(7) Kang, D. Y.; Moon, J. K. Carbon Nanotube Balls and Their Application in Supercapacitors. *ACS Appl. Mater. Interfaces* **2014**, *6*, 706−711.

(8) Huang, C.; Grant, P. S. One-Step Spray Processing of High Power All-Solid-State Supercapacitors. *Sci. Rep.* **2013**, *3*, 1−9.

(9) Chen, T.; Peng, H.; Durstock, M.; Dai, L. High-Performance Transpatrent and Stretchable All-Soild Supercapacitors Based on Highly Aligned Carbon Nanotube Sheet. *Sci. Rep.* **2014**, *4*, 1−7.

(10) Tans, S. J.; Verschueren, A. R. M.; Dekker, C. Room-Temperature Transistor Based on a Single Carbon Nanotube. *Nature* **1998**, *393*, 49−52.

(11) Javey, A.; Kim, H.; Brink, M.; Wang, Q.; Ural, A.; Guo, J.; Mcintyre, P.; Lundstrom, M.; Dai, H. High-*k* Dielectrics for Advanced Carbon Nanotube Transistors and Logic Gates. *Nat. Mater.* **2002**, *1*, 241−246.

(12) Javey, A.; Guo, J.; Wang, Q.; Lundstrom, M.; Dai, H. Ballistic Carbon Nanotube Field-Effect Transistors. *Nature* **2003**, *424*, 654−657.

(13) Chae, S. H.; Yu, W. J.; Bae, J. J.; Duong, D. L.; Perello, D.; Jung, H. Y.; Ta, Q. H.; Ly, T. H.; Vu, Q. A.; Yun, M. H.; Duan, X.; Lee, Y. H. Transferred Wrinkled Al_2O_3 for Highly Stretchable and Transparent Graphene-Carbon Nanotube Transistors. *Nat. Mater.* **2013**, *12*, 403−409.

(14) Ajayan, P. M.; Tour, J. M. Nanotube Composites. *Nature* **2007**, *447*, 1066−1068.

(15) Gavalas, V. G.; Andrews, R.; Bhattacharyya, D.; Bachas, L. G. Carbon Nanotube Sol-Gel Composite Materials. *Nano Lett.* **2001**, *1*, 719−720.

(16) Meng, F.; Zhang, X.; Xu, G.; Yong, Z.; Chen, H.; Chen, M.; Li, Q.; Zhu, Y. Carbon nanotube Composite Films with Switchable Transparency. *ACS Appl. Mater. Interfaces* **2011**, *3*, 658−661.

(17) Shulaker, M. M.; Hills, G.; Patil, N.; Wei, H.; Chen, H.; Wong, H. − S. P.; Mitra, S. Carbon Nanotube Computer. *Nature* **2013**, *501*, 526−530.

(18) Kang, W.; Kim, N. H.; Lee, D. Y.; Chang, S. T.; Cho, J. H. Micropatterned Single-Walled Carbon Nanotube Electrodes for Use in High-Performance Transistors and Inverters. *ACS Appl. Mater. Interfaces* **2014**, *6*, 9664−9670.

(19) Yu, D.; Dai, L. Self-Assembled Graphene/Carbon Nanotube Hybrid Films for Supercapacitors. *J. Phys. Chem. Lett.* **2010**, *1*, 467−470.

(20) Di, J.; Hu, D.; Chen, H.; Yong, Z.; Chen, M.; Feng, Z.; Zhu, Y.; Li, Q. Ultrastrong, Foldable, and Highly Conductive Carbon Nanotube Film. *ACS Nano* **2012**, *6*, 5457−5464.

(21) Jo, J. W.; Jung, J. W.; Lee, W. J.; Jo, W. H. Fabrication of Highly Conductive and Transparent Thin Films from Single-Walled Carbon Nanotubes Using a New Non-ionic Surfactant *via* Spin Coating. *ACS Nano* **2010**, *4*, 5382−5388.

(22) Wang, J.; Zhang, J.; Sundramoorthy, A. K.; Chen, P.; Chan-Park, M. B. Solution-Processed Flexible Transparent Conductors Based on Carbon Nanotubes and Silver Grid Hybrid Films. *Nanoscale* **2014**, *6*, 4560−4565.

(23) Han, J. T.; Kim, D.; Kim, J. S.; Seol, S. K.; Jeong, S. Y.; Jeong, H. J.; Chang, W. S.; Lee, G. W.; Jung, S. Self-Passivation of Transparent Single-Walled Carbon Nanotube Films on Plastic Substrates by Microwave-Induced Rapid Nanowelding. *Appl. Phys. Lett.* **2012**, *100*, 163120−1−163120−4.

(24) Aliev, A. E.; Lima, M. D.; Fang, S.; Baughman, R. H. Underwater Sound Generation Using Carbon Nanotube Projectors. *Nano Lett.* **2010**, *10*, 2374−2380.

(25) Chen, T.; Qiu, L.; Cai, Z.; Gong, F.; Yang, Z.; Wang, Z.; Peng, H. Interwined Aligned Carbon Nanotube Fiber Based Dye-Sensitized Solar Cells. *Nano Lett.* **2012**, *12*, 2568−2572.

(26) Aykol, M.; Hou, B.; Dhall, R.; Chang, S.; Branham, W.; Qiu, J.; Cronin, S. B. Clamping Instability and van der Waals Forces in Carbon Nanotube Mechanical Resonators. *Nano Lett.* **2014**, *14*, 2426−2430.

(27) Kim, B.; Lu, Y.; Kim, T.; Han, J.; Meyyappan, M.; Li, J. Carbon Nanotube Coated Paper Sensor for Damage Diagnosis. *ACS Nano* **2014**, *8*, 12092−12097.

(28) Luo, S.; Liu, T. Structure−Property−Processing Relationships of Single-Wall Carbon Nanotube Thin Flm Piezoresistive Sensors. *Carbon* **2013**, *59*, 315−324.

(29) Kim, S. K.; Wang, X.; Ando, S.; Wang, X. Low Dielectric and Thermally Stable Hybrid Ternary Composites of Hyperbranched and Linear Polyimide with SiO_2. *RSC Adv.* **2014**, *4*, 27267−27276.

(30) Kim, S. K.; Wang, X.; Ando, S.; Wang, X. Hybrid Ternary Compoistes of Hyperbranched and Linear Polyimides with SiO_2: A

DOI: 10.1021/acsami.5b06181
ACS Appl. Mater. Interfaces 2015, 7, 20865−20874

Research for Low Dielectric Constant and Optimized Properties. *RSC Adv.* **2014**, *4*, 42737−42746.
(31) Kim, S. K.; Ando, S.; Wang, X. Thernary Composites of Linear and Hyperbranched Polyimides with Nanoscale Silica for Low Dielectric Constant, High Transparency, and High Thermal Stability. *RSC Adv.* **2015**, *5*, 40046−40054.
(32) Kim, S. K.; Wang, X.; Ando, S.; Wang, X. Highly Transparent Triethoxysilane-Terminated Copolyimide and Its SiO_2 Composite with Enhanced Thermal Stability and Reduced Thermal Expansion. *Eur. Polym. J.* **2015**, *64*, 206−214.
(33) Lewis, J. Materials Challenge for Flexible Organic Devices. *Mater. Today* **2006**, *9*, 38−45.
(34) Liu, T.; Xiao, Z.; Wang, B. The Exfoliation of SWCNT Bundles Examined by Simultaneous Raman Scattering and Photoluminescence Spectroscopy. *Carbon* **2009**, *47*, 3529−3537.
(35) Luo, S.; Liu, T.; Wang, B. Comparison of Ultrasonication and Microfluidization for High Throughput and Large-scale Processing of SWCNT Dispersions. *Carbon* **2010**, *48*, 2992−2994.
(36) Liu, T.; Luo, S.; Xiao, Z.; Zhang, C.; Wang, B. Preparative Ultracentrifuge Method for Characterization of Carbon Nanotube Dispersions. *J. Phys. Chem. C* **2008**, *112*, 19193−19202.
(37) Jeong, H.; Park, J. Y. Local Electrical Investigations of Nitric Acid Treatment Effects on Carbon Nanotube Networks. *J. Phys. Chem. C* **2015**, *119*, 9665−9668.
(38) Hu, L.; Hecht, D. S.; Grüner, G. Percolation in Transparent and Conducting Carbon Nanotube Networks. *Nano Lett.* **2004**, *4*, 2513−2517.
(39) Luo, S.; Liu, T.; Benjamin, S. M.; Brooks, J. S. Variable Range Hopping in Single-Wall Carbon Nanotube Thin Films: A Processing−Structure−Property Relationship Study. *Langmuir* **2013**, *29*, 8694−8702.
(40) Harris, J. M.; Swathi lyer, G. R.; Bernhardt, A. K.; Huh, J. Y.; Hudson, S. D.; Fagan, J. A.; Hobbie, E. K. Electronic Durability of Flexible Transparent Films from Type-Specific Single-Wall Carbon Nanotubes. *ACS Nano* **2012**, *6*, 881−887.
(41) Zhao, S.; Zhang, G.; Gao, Y.; Deng, L.; Li, J.; Sun, R.; Wong, C. P. Strain-Driven and Ultrasensitive Resistive Sensor/Switch Based on Conductive Alginate/Nitrogen-Doped Carbon-Nanotube-Supported Ag Hybrid Aerogels with Pyramid Design. *ACS Appl. Mater. Interfaces* **2014**, *6*, 22823−22829.
(42) Khaligh, H. H.; Goldthorpe, I. A. Failure of Silver Nanowire Transparent Electrodes under Current Flow. *Nanoscale Res. Lett.* **2013**, *8*, 235.

DOI: 10.1021/acsami.5b06181
ACS Appl. Mater. Interfaces 2015, 7, 20865−20874